J. Chem. Soc., Faraday Trans. 1, 1987, **83**, 1063–1079

Experimental Evaluation of Adsorption Behaviour of Intermediates in Anodic Oxygen Evolution at Oxidized Nickel Surfaces

Brian E. Conway* and Tongchang Liu†

Chemistry Department, University of Ottawa, 365 Nicholas Street, Ottawa K1N 9B4, Ontario, Canada

By means of digital acquisition and processing of potential-decay transients, following interruption of anodic currents for O_2 evolution at oxidized Ni surfaces, the behaviour of the adsorbed intermediate species in the heterogeneous reaction is quantitatively evaluated for various initial currents and for several temperatures. The method is of interest in electrocatalysis and electrode kinetics since it provides, by its nature, information on the adsorbed species that are kinetically involved as intermediates in the steady state of the reaction proceeding at appreciable net rates, rather than on some strongly bound species that may be adsorbed but not participate as the active intermediate in the reaction sequence. The behaviour of the O_2 evolution reaction at oxidized Ni anodes is characterized by two regions of potential-dependent pseudocapacitance that reflect the potential dependence of the surface density of the intermediate species: one probably involving the surface region of the nickel oxide film and another involving a potential-dependent state of oxidation of bulk-phase-type oxide. The behaviour of the adsorbed intermediates, OH or O, is intimately connected with the oxidation states of Ni as Ni^{3+} and Ni^{4+} in the surface region of the oxide film at which O_2 is anodically evolved. Experiments at various temperatures reveal an important dependence of the adsorption behaviour of the intermediates on that variable; the effect arises for kinetic reasons.

In studies of the mechanisms and polarization behaviour of electrode reactions, the role of intermediates is of major interest. This is specially the case for multistep processes in electrocatalysis and catalysis that involve intermediates that are chemisorbed[1–4] or participate through some special oxidation state of the surface,[5] as in anodic reactions involving oxide films.[6] In most cases of multistep electrode reactions there is dependence on electrode potential of the steady-state coverage by the electroactive intermediate(s), as for H in the H_2 evolution reaction[7, 8] (h.e.r.). This dependence determines the Tafel slope, b, of the process and hence the polarization performance of the electrode reaction; thus, a low b value is as important as a high exchange current density, especially as a requirement for low polarization 'super-electrodes'[7, 9] that give overpotentials no greater than *ca.* 100 mV at current densities *ca.* 0.1 A cm^{-2}. This matter is therefore of practical importance in such problems as optimization of performance of advanced water electrolysers for H_2 production. Hitherto, surprisingly little information exists on the kinetic and electrochemical adsorption behaviour of the electroactive intermediates that are the kinetically involved species in Faradaic reactions proceeding at appreciable currents and corresponding overpotentials, although this information is essential for an experimentally based interpretation of kinetics and mechanism of various electrode processes and, in general, of electrocatalysis and regular heterogeneous catalysis.

† On leave of absence from the People's Republic of China.

On the other hand, the strongly bound species that arise in underpotential deposition have been well characterized by means of cyclic voltammetry,[10, 11] galvanostatic charging experiments,[12, 13] a.c. impedance and relative reflectivity measurements. Only in some early papers by Breiter *et al.*,[14, 15] Gerischer and Mehl[16] and Bockris *et al.*[17] were some attempts made to study the behaviour of overpotential-deposited (o.p.d.) species, *e.g.* H in the h.e.r. More recently, a new approach was developed by Conway and Bai,[7] using analysis of digitally recorded potential-decay curves, which gave full information on potential dependence of H coverage in the h.e.r. over a wide range of cathodic current densities at Ni[7, 9] Pt,[18] Au[19] and Ni–Mo alloy[7, 9] electrodes. These results enabled the Tafel-slope behaviour of the h.e.r. at these metals to be rationalized for the first time in terms of the experimentally evaluated potential dependence of H coverage, θ, and the corresponding pseudocapacitance, C_ϕ, at appreciable overpotentials.

With regard to the well known problem of characterization of adsorbed species in heterogeneously catalysed reactions, it is important to note that the potential-decay method, by its intrinsic nature, gives information on the coverage by the ad-species that are the actual kinetically involved intermediates in the steady state or quasi-steady state of the reaction. This is an advantage peculiar to methods applicable to electrode reactions; no corresponding approach is available, to our knowledge, for ordinary heterogeneously catalysed reactions. Spectroscopic, *e.g.* i.r., methods have been used, but these do not necessarily characterize the short-lived species that are the true intermediates in the kinetics of the catalysed process.

The potential decay method[20–22] for evaluation of the behaviour of adsorbed intermediates in electrode reactions has the advantages that: (*a*) prior knowledge or assumptions about the reaction mechanism are not required; (*b*) no empirical quantities, *e.g.* the integration constant when eqn (1) (see below) is integrated [*cf.* ref. (5)], are required for evaluation of the quantities C_ϕ or coverage, θ, of the intermediates and (*c*) the method is applicable over a wide range of overpotentials and corresponding Faradaic currents for the reaction being studied, when its current efficiency is near 100%.

For the anodic O_2 reaction (o.e.r.), on the other hand, despite interesting theoretical discussions of the kinetic role of OH and O intermediates in the o.e.r.[3] and the state of O_2-evolving anodes bearing oxide films,[6] virtually no experimental information on the behaviour of the adsorbed intermediates is available.

The first use of the potential-decay method for study of O_2 evolution processes was made by Conway and Bourgault[5, 20] at nickel oxide battery plaque electrodes. Recently[23, 24] Willems *et al.* have used this procedure, coupled with impedance measurements, to study the o.e.r. at Co and $La_{0.5}Ba_{0.5}CoO_3$. At the former material, the o.e.r. behaviour has some features similar to those of the reaction at nickel oxide.[5, 20]

In the present paper we show how application of the recently developed potential-decay method[7] to study of the o.e.r. at oxidized Ni anode surfaces enables quantitative information to be obtained on the potential dependence of the coverage of the oxide surface at Ni by the o.p.d. intermediates involved in the o.e.r. proceeding at appreciable current densities for O_2 evolution. The observed adsorption behaviour is related to the electrochemical kinetics of the process at several temperatures and to the state of oxidation of Ni ions in the surface region of the oxide film.

Experimental

Systems

The behaviour of the anodic O_2 evolution reaction on Ni electrodes bearing thin, anodically formed oxide films was studied. The electrochemical characteristics of this film were determined by means of cyclic voltammetry. The oxide film was grown anodically at 298 K for 1 h at 0.57 V *vs.* Hg/HgO in 1 mol dm^{-3} aqueous recrystallized NaOH.

Method

The potential-decay method originates from the work of Butler and Armstrong[25] and Morley and Wetmore.[21] Conway and Bourgault[20] showed how it could usefully be applied to interpretation of electrode reaction mechanisms through the potential dependence of adsorption pseudocapacitance[26] of the electroactive intermediate involved in a Faradaic reaction. The method provides information complementary to that obtainable by a.c. impedance measurements.

Experimental aspects of a new embodiment of the method have been described elsewhere in some detail by Conway *et al.*[27] and by Conway and Bai[7] in application to the H_2 evolution reaction. The approach used involves digital data collection through a Nicolet oscilloscope[27] and processing by means of a computer to obtain (*a*) the adsorption pseudocapacitance, C_ϕ, of the o.p.d. species as a function of overpotential, η; (*b*) η *vs.* log(time) curves for the potential decay and (*c*) η *vs.* $\ln(-\mathrm{d}\eta/\mathrm{d}t)$ relations.[28] These three functions give a complete account of the potential dependence of adsorption of intermediates in the kinetics and mechanism of the reaction if the Tafel polarization relation, η *vs.* $\log i$, has also been accurately evaluated under the same conditions [cf. ref. (7)].

Theoretical aspects of potential-decay behaviour, following interruption of polarization, were given by Tilak and Conway[22] for several electrode reaction mechanisms of the type that involve chemisorbed intermediates, and the steady-state pseudocapacitance of intermediates involved in continuous Faradaic reactions was treated by Gileadi and Conway.[26c]

In the present work the instrumental arrangement and procedure were the same as described in previous papers[7, 9, 27] on the h.e.r., and as referred to in a general way above. η *vs.* t transients, following interruption of anodic polarization at various current densities, i, were recorded digitally over 5 to 6 decades of t by means of two digital oscilloscopes in tandem. Each transient was recorded with *ca.* 8000 data points. η *vs.* $\ln i$ relations were determined over several decades of i with 20 points per decade. The results were processed as described previously[7, 27] for the h.e.r. experiments.

Reference Electrodes

Hg/HgO reference electrodes, made up with the same NaOH electrolyte as used in the kinetic runs, were used in all the experiments, as described in ref. (5). In experiments over a range of temperatures, the Hg/HgO electrode was kept at the same temperature as the Ni working electrode. Potentials are expressed as V/V *vs.* the Hg/HgO electrode in the figures which follow. The O_2 overpotentials η are then $V - 0.306$ V.

Results and Discussion

Cyclic Voltammetry of Film Formation and Reduction

The anodic oxide films at Ni wire electrodes on which the O_2 evolution process was studied are characterized electrochemically by the cyclic voltammograms in fig. 1 for oxide formation and reduction (to the Ni^{II} oxidation state). The cathodic profiles always consist of two overlapping peaks, as known previously. The oxidation and reduction charges were 2.94 ± 0.12 and 2.90 ± 0.10 mC cm^{-2}, respectively, based on averages of data for three electrodes examined at three sweep-rates of 50, 100 and 200 mV s^{-1}. For three electrodes at 100 mV s^{-1} the results for the oxidation/reduction charges were reproducible to 0.04 mC cm^{-2}; these charges correspond to oxidation of an initial film of $Ni(OH)_2$ to higher oxidation states (Ni·O·OH, 'NiO_2'), and corresponding reduction back to $Ni(OH)_2$. The current peaks in fig. 1 do not correspond to oxidation from or

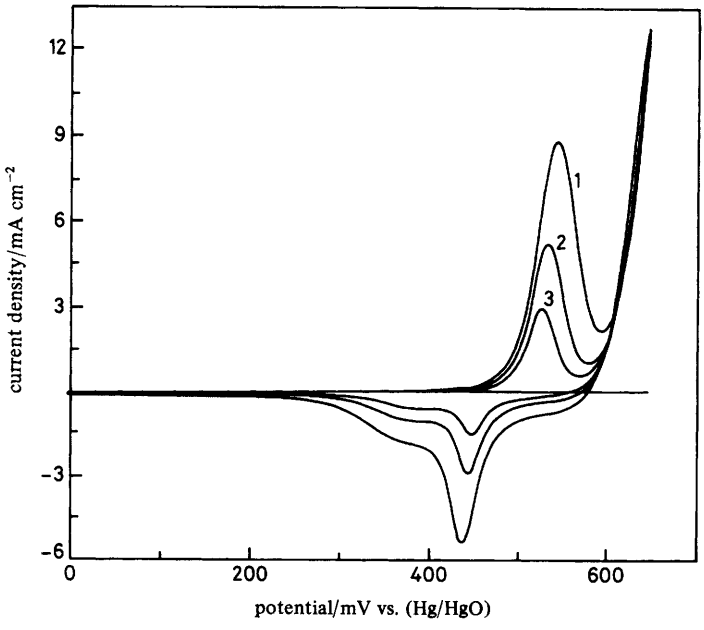

Fig. 1. Cyclic-voltammetry current *vs.* potential curves for the oxide film at Ni electrodes in 0.2 mol dm^{-3} NaOH at 299 K at sweep-rates of (3) 50; (2) 100 and (1) 200 mV s^{-1}.

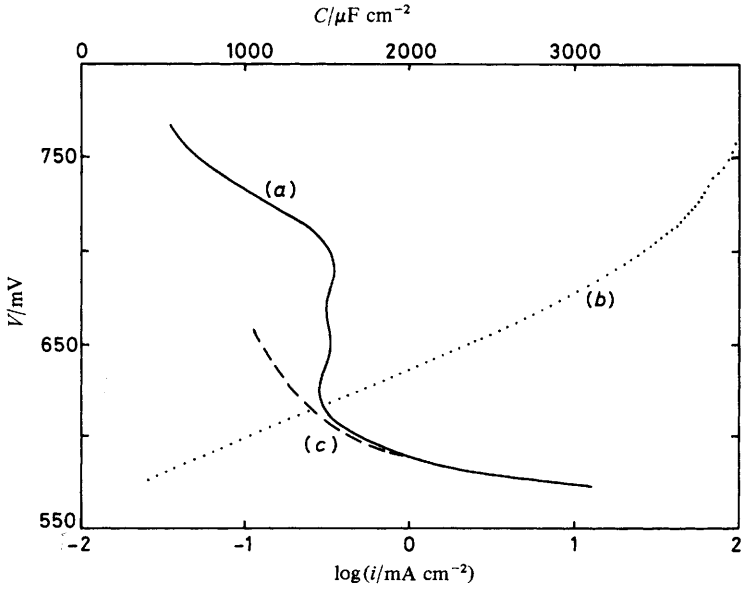

Fig. 2. (···) Tafel relation for O_2 evolution at the oxidized Ni electrode at 298 K in 0.2 mol dm^{-3} NaOH. Superimposed is one of the $C(V)$ relations from fig. 6 (——). The dashed region indicates probable trend of bulk oxide $C(V)$ component based on fig. 1.

reduction to the Ni^{O} oxidation state, which are highly irreversible processes at ordinary temperatures.

The oxide film thicknesses were estimated to be equivalent to *ca.* 11 layers, based on an initial roughness factor of *ca.* 1.6 for the underlying metal and a charge required for one-electron oxidation of a monolayer of $Ni(OH)_2$ of 270 $\mu C\ cm^{-2}$. The exact value of the oxide film thickness is not, however, required for any of the quantities that are derived in subsequent sections of this paper.

For the potential-decay experiments the oxide films were formed for 1 h at a controlled potential, and the potential was then held constant for 30 s, at several values along the Tafel relation characterizing the polarization behaviour of the o.e.r. (fig. 2). In some experiments a longer anodic holding time was used. Under the SEM the anodic oxide films at Ni are featureless except for reproduction of some initial non-uniformities on the original metal surface.

Log (Current) *vs.* Potential and Potential-decay Relations

Log (current-density, i) *vs.* potential relations for the o.e.r. at the anodically oxidized Ni electrodes were recorded potentiostatically in 0.2 mol dm^{-3} aqueous NaOH, as shown typically in fig. 2. Potential-decay transients were taken from various anodic potentials along the Tafel line upon interruption of successively established, steady anodic currents as shown in fig. 3 for six current densities for O_2 evolution from 8 to 100 mA cm^{-2}; the electrode potential is plotted in $\log t$ [fig. 3(*a*)] during the potential decay [*cf.* ref. (20), (21) and (27)]. These curves became almost superimposed upon plotting the same data in $\log(t+\tau)$ [fig. 3(*b*)], where τ is the integration constant[20, 21] of the integrated decay-rate equation[20, 21]

$$-C\frac{d\eta}{dt} = -(C_\phi + C_{dl})\,d\eta/dt = i(\eta) = i_0 \exp[\alpha\eta(t)\,\boldsymbol{F}/\boldsymbol{RT}] \qquad (1)$$

in which $i(\eta)$ is the current *vs.* potential function for the o.e.r., i_0 its exchange current density and α its transfer coefficient.

In using eqn (1) it is to be noted that no 'iR' correction enters into the right-hand term, since eqn (1) applies to open-circuit conditions after current interruption, and the initial 'vertical drop' of the $\eta(t)$ transient in fact allows a separate evaluation of any iR drop at each current, giving data by which the Tafel polarization relations were corrected, where necessary, for any iR drop effects. Also [*cf.* ref. (7) and (9)], no corrections for back-reaction currents near the reversible potential in the decay transient are required, since it is the net self-discharge current that determines the depolarization of the double layer leading to the decay transient.

In eqn (1) C is the total electrode capacitance[7, 22] associated with the process, in particular being comprised of the double-layer capacitance, C_{dl}, and the pseudocapacitance,[26] C_ϕ, associated with potential dependence of the surface density of intermediates in the o.e.r. at the oxide film interface. The relation between C_ϕ, C_{dl} and eqn (1) to the equivalent circuit for open-circuit decay processes has been referred to in ref. (7), (18) and (22), and will be treated in more detail in ref. (29).

The decay data may also be processed directly in terms of $d\eta/dt$ or $\log(-d\eta/dt)$,[27, 28] giving information on potential dependence of C. Plots of $\eta(t)$ *vs.* $\log(-d\eta/dt)$ are shown in fig. 4 for the six current densities corresponding to data in fig. 3. The slopes of the lower potential regions are *ca.* 28 mV, and those of the upper regions *ca.* 58 mV, *i.e. ca.* twice as large.

Comparison of the Tafel relation $\eta(i)$ *vs.* $\log i$ and (see fig. 5) the potential-decay plots, $\eta(t)$ *vs.* $\log(-d\eta/dt)$, gives a basis for estimation of C_{dl} when the two types of plots exhibit parallel regions, *i.e.* when $C_\phi \to 0$ (for $\theta \to 0$ or $\to 1$) and C is then determined principally by C_{dl}. The separation of the two types of plots in the parallel region on the

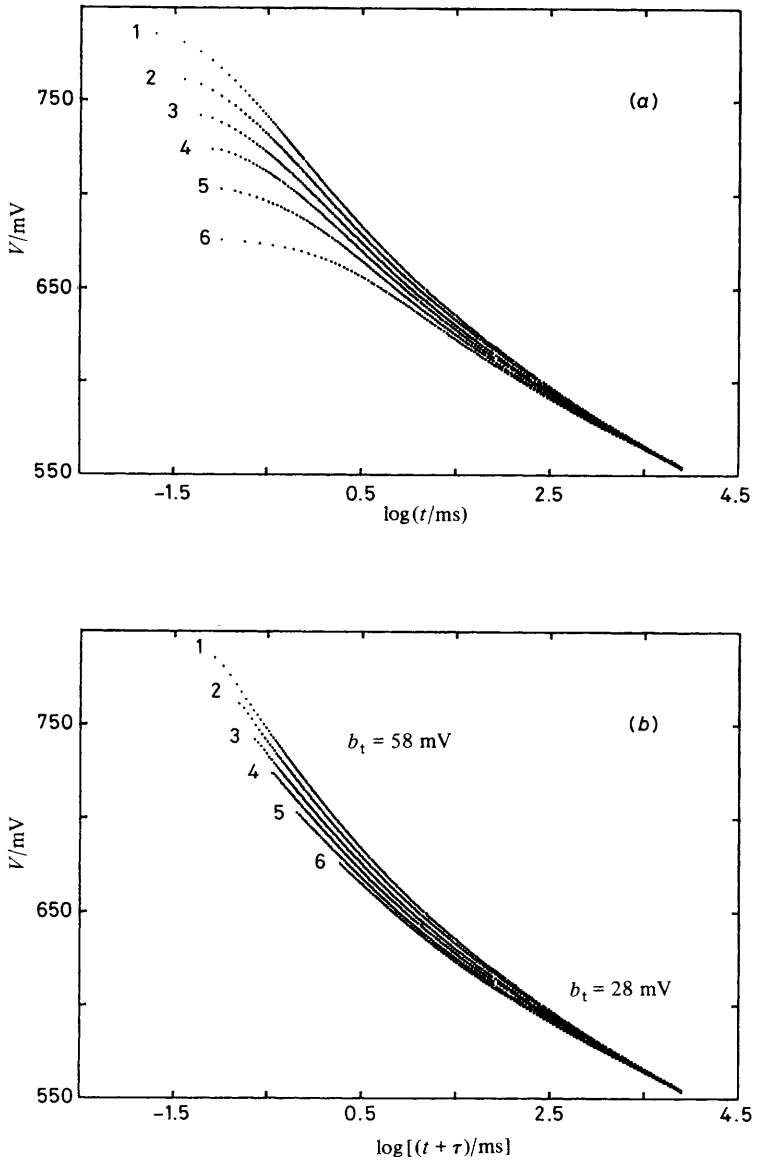

Fig. 3. Potential-decay transients, digitally recorded, plotted (*a*) *vs.* $\log(t/\text{ms})$ and (*b*) *vs.* $\log[(t+\tau)/\text{ms}]$ for six current densities of anodic O_2 evolution. (1) 100; (2) 80, (3) 61, (4) 43, (5) 23 and (6) 8 mA cm^{-2}. $T = 299$ K.

same log scale then gives $\log C_{dl}$, as follows from eqn (1) when C is written as $C_{dl}+C_\phi$ with $C_\phi \rightarrow 0$ for the approach to surface saturation (or constant coverage[7]) by the adsorbed intermediates.[26]

It was shown in separate experiments[19] on decay of cathodic polarization at Au, as a test of the potential-decay method, that the correct double-layer capacity behaviour for Au is recovered with $C_{dl} = 24$ μF cm^{-2} over a potential range of 0.45 V, independent of potential, in agreement with results from cyclic voltammetry.

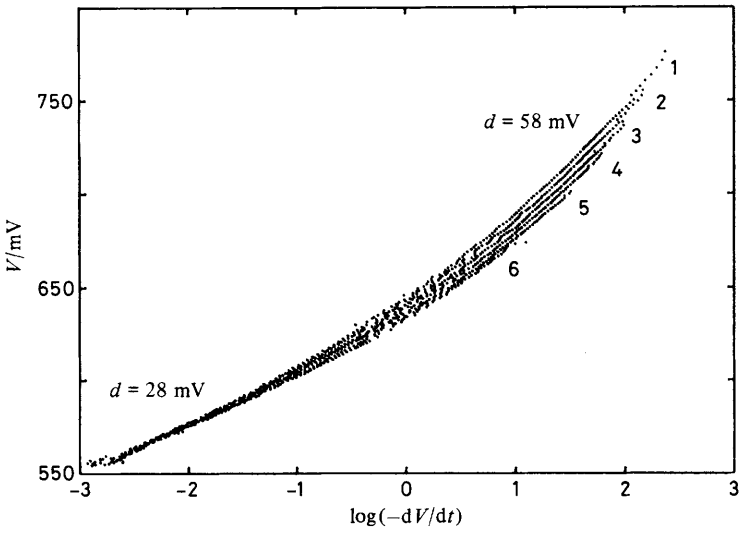

Fig. 4. Plots of $\log(-\mathrm{d}V/\mathrm{d}t)$ *vs.* electrode potential during decay transients taken from various initial potentials at six corresponding current densities (as for fig. 3) for anodic O_2 evolution at oxidized Ni electrodes.

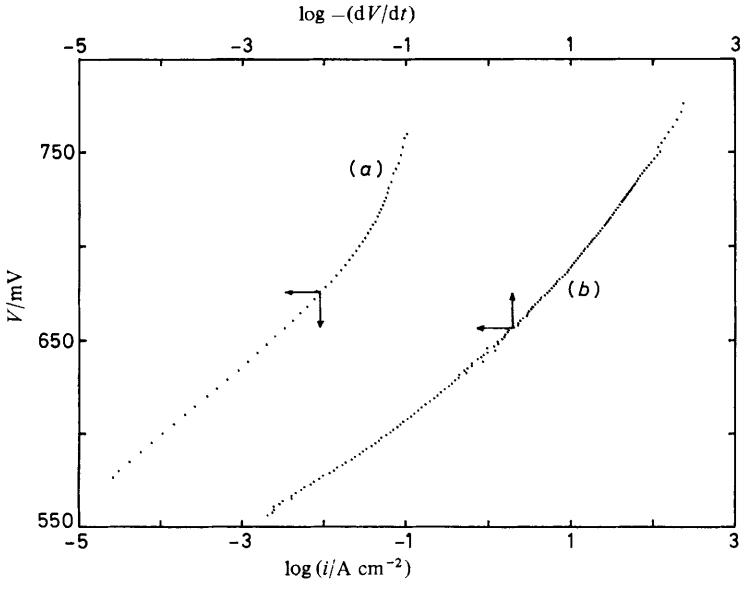

Fig. 5. Comparison of (*a*) the Tafel relation for O_2 evolution and (*b*) the $\ln(-\mathrm{d}V/\mathrm{d}t)$ *vs.* η relation obtained under the same conditions ($T = 299$ K, initial current density 100 mA cm^{-2}).

Evaluation of Pseudocapacitance and Coverage Behaviour of the Adsorbed Species in the O.E.R. at Anodic Oxide Films at Ni

Intermediates in the O_2 evolution reaction were regarded in the early work as simply OH or O species chemisorbed at the electrode metal.[3] However, the latter situation probably only obtains for quite low coverages of u.p.d. OH species, 5–10% of a monolayer, at

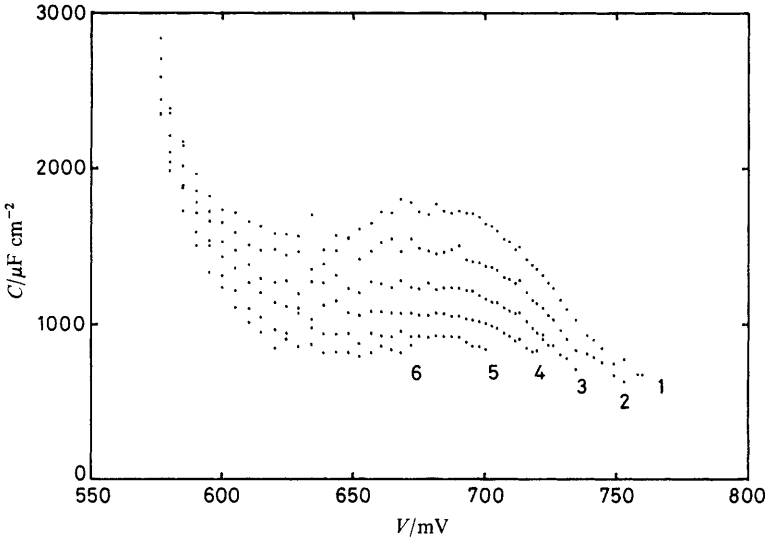

Fig. 6. Profiles of $C_\phi + C_{dl}$ as a function of potential for the O_2 evolution reaction at oxidized Ni electrodes derived from the potential-decay transients of fig. 3 taken from the six initial anodic current densities for O_2 evolution listed in fig. 3. Curve labelling as in fig. 3 for the six current densities.

noble metals such as Pt or Au,[4,10] prior to O_2 evolution. At all metals, oxygen evolution is preceded by formation of a three-dimensional oxide film (or a quasi-three-dimensional reconstructed O/metal film, as is the case at *e.g.* Au or Pt) on which the process of OH and/or O discharge takes place. This can be considered as equivalent to a local formation of an higher oxidation state of the metal ion of the oxide-film lattice at its surface, *e.g.* at oxide films on Ni, Co, Au, Pt *etc.*

This situation can be represented as follows in terms of surface elements of the Ni^{3+}/Ni^{4+} oxide lattice for potentials $>$ *ca.* 0.58 V *vs.* Hg/HgO:

$$\begin{matrix} & OH^- & & OH^- & & OH^- \\ Ni^{3+}, & O^{2-} + OH^- \rightarrow & Ni^{3+} & OH^{\cdot} & + e \leftrightarrow Ni^{4+} & OH^- \\ & & & O^{2-} & & O^{2-} \end{matrix} \qquad (2)$$

as was proposed by Conway and Bourgault[5] and treated in a related way in later papers by Trasatti *et al.*[6]

From eqn (1), $C(\eta)$ can be evaluated over the range of potentials for which the potential-decay and polarization behaviour have been measured under the same experimental conditions. Integration of the resulting relation between $C(\eta)$ and η then gives the surface density or coverage (or the changes in these quantities) of the intermediates over the studied potential range for the Faradaic reaction investigated. The C data and resulting coverage information, it is to be noted, refer to the species kinetically involved in the process of active Faradaic evolution of O_2 at the various current densities covered in the Tafel plot. We have referred to such intermediates as the 'overpotential-deposited' (o.p.d.) species[7] of the Faradaic reaction to distinguish them from u.p.d. species that may be deposited before onset of the net continuous Faradaic reaction (*i.e.* below its reversible potential), *e.g.* at Pt or Au.

A typical profile of capacitance, $C(\eta)$, derived as a function of η from eqn (1) is shown in fig. 2. Fig. 6 shows a series of $C(\eta)$ profiles for the decay data obtained at six current densities (fig. 3) along the curve of fig. 2. It is clear that two regions of the $C(\eta)$ relation

arise: one, an ascending region of C values with decreasing η, below *ca.* 0.64 V *vs.* Hg/HgO and a second, exhibiting a maximum between 0.64 and 0.75 V *vs.* Hg/HgO; also the $C(\eta)$ profiles, although of the same general shape, depend appreciably, in the magnitudes of C, on the current density of prior steady-state polarization in the range 8–100 mA cm^{-2}. Note that all these $C(\eta)$ data refer to the region beyond (>0.6 V) the anodic peaks of the cyclic voltammograms of fig. 1, *i.e.* where active anodic O_2 evolution is taking place in the o.p.d. region. (The peaks in fig. 1 are not, however, to be regarded as referring to corresponding u.p.d. processes in the usual sense of the term but rather to a change of oxidation state of the material in the oxide film. However, it is this change of oxidation state of the oxide, manifested at its surface, that eventually leads to a situation where, at a sufficient potential, O_2 evolution can proceed at appreciable rates on the oxide surface.)

Effect of Anodic Polarization Current Density

For a simple process, not involving a change of state of the electrode with current density or corresponding overpotential, the plots of η *vs.* $\log(t+\tau)$ or η *vs.* $\log(-\mathrm{d}\eta/\mathrm{d}t)$ are expected to be independent of the prior polarization conditions, *i.e.* they are superimposable. This is observed for some systems, *e.g.* cathodic H_2 evolution on Hg, Au or Ni. In the present case, for the o.e.r., there is some small but significant dependence of the potential-decay behaviour on prior polarization current density as seen in fig. 3 and 4. Since in fig. 4 no problem of empirical evaluation of the integration constant τ arises, as it does in plotting the data of fig. 3 as $f[\log(t+\tau)]$, the differences revealed in the former figure for the various anodic current densities reflect a real effect of the initial state of the electrode at the six current densities. This is understandable since the state of oxidation of the anodic oxide film on the Ni anodes is expected [*cf.* ref. (20)] to be dependent on the anodic O_2 evolution current density and the corresponding overpotential.

From the corresponding pseudocapacity behaviour derived for the electrode polarized at the six current densities, shown in fig. 6, it is evident that the derived C_ϕ *vs.* η behaviour is quite dependent on the prior anodic polarization current density or potential, although, as noted above, the general forms of the curves are rather similar to one another.

The C_ϕ *vs.* η behaviour seems to be compounded of one component that decreases continuously from high values at low potentials (<0.575 V) and a second, of comparable magnitude, that exhibits a maximum around 0.675 V.

In relation to the cyclic-voltammetry profiles of fig. 1, it seems that the former component may be due to the pseudocapacitance of the 'bulk' material of the oxide film (reflecting its oxidation/reduction state as a function of potential below 0.60 V), while the second component in C_ϕ, showing the maximum, represents the behaviour of the more highly oxidized surface states of the oxide film associated with the o.p.d. intermediates of the Faradaic oxygen evolution reaction. Evidently the process/species giving rise to the maximum between *ca.* 0.625 and 0.75 V provides a progressively smaller contribution to C_ϕ as the polarization current density decreases from 100 to 8 mA cm^{-2} in the series of potential-decay transients (fig. 3) recorded. This is understandable if this species is identified with the more highly oxidized surface states, Ni^{IV}, of the oxide film or equivalently to the deposition of $OH^{\cdot}$ at the oxide surface [eqn (2)].

A similar distinction between the behaviour of bulk $NiO \cdot OH$ material, with Ni in the (III) oxidation state, and a surface region in a higher, (IV), oxidation state was indicated in our earlier work[20] on the mechanism of charging and coupled O_2 evolution on nickel oxide in Ni battery positive plates where the oxide is present in bulk form as a wetted powder. At Co, a similar, more highly oxidized surface region of CoO_2, was also proposed[23] recently.

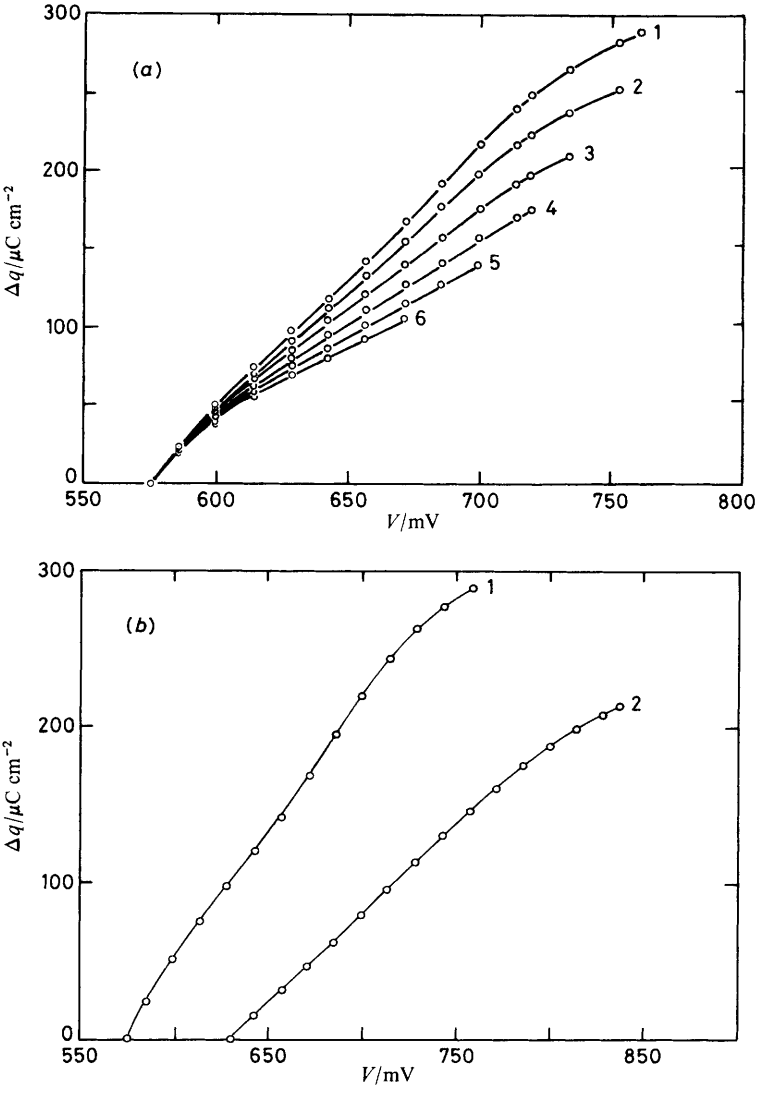

Fig. 7. (*a*) Charge plots, Δq *vs.* electrode potential, for the change of steady-state surface density of reaction intermediates in the o.e.r. at oxidized Ni electrodes for the same six initial O_2 evolution current densities of fig. 3 (data derived from transients of fig. 3 through the C values of fig. 6). (*b*) As in (*a*) for two temperatures: (1) 299 and (2) 273.6 K.

Charge *vs.* Potential Relationships

From the C_ϕ *vs.* η plots, it is easy to calculate by integration the charge, Δq, corresponding to change of state of the surface, for various steady-state rates of the o.e.r. over the potential range covered in the potential-decay transients.

Electrochemical charge isotherm plots for Δq as $f(\eta)$ are shown in fig. 7 for several initial states of the O_2-evolving nickel oxide films, *i.e.* for several initial current densities of O_2 evolution. It is seen from fig. 7(*a*) and (*b*) that Δq approaches values between

200 and 300 μC cm^{-2} when C is integrated from the highest potentials. These values correspond to a surface density of 'one-electron' species near that equivalent to a monolayer of o.p.d. intermediates.

During O_2 evolution, where charge passes continuously according to the Faradaic production of O_2 requiring 4 F per mol of O_2, the above charge, Δq, corresponds to the change of 'steady-state' surface concentration of adsorbed OH or O intermediates (or of corresponding Ni^{4+}, Ni^{3+} surface states of the oxide film[5]) as the self-discharge Faradaic reaction of O_2 evolution decreases in rate on open circuit with fall of potential. Similarly, a change of state of the oxide arises, especially at and near its surface, as O_2 evolution is caused to proceed at different current densities and potentials in a polarization experiment.

In the case of O_2 evolution at nickel oxide, or at other similar oxides, *e.g.* of Co,[23] where mixed oxidation states can develop as electrode potential is changed, the interpretation of the effects of changing potential either in the polarization curve or on open circuit is more complicated than with the H_2 evolution reaction.[7, 8] In the latter case the substrate metal remains invariant (except perhaps when hydride formation can occur[7, 18] in parallel with H_2 evolution) with change of potential. In the o.e.r. case, however, the oxidation state of the oxide can vary both at its surface and in its bulk, with potential, in the course of evolution of O_2 at various overpotentials or on open circuit. This is because, with Ni and some other mixed-valency oxides, there can be a progressive change of average oxidation state over the potential range of appreciable rates of O_2 evolution up to the potential where the highest oxidation state of the oxide is reached (NiO_2, CoO_2 and IrO_2). There can thus arise a close relation between the coverage of the oxide film by OH and O intermediates of the o.e.r. and the state of oxidation of nickel ion species at the oxide's interface, as we have implied earlier[5] [see eqn (2)].

Usually the high oxidation states of such oxides are unstable in water so, in the absence of polarization associated with O_2 evolution, they will decompose through a mixed cathodic/anodic self-discharge process[5] with accompanying O_2 evolutions[5, 30] and suffer a decrease of their oxidation state until the redox potential of the oxide matches the O_2 reversible potential or some stationary mixed potential is attained.

Probably, as was shown in ref. (5) for Ni oxide and indicated now also for the Co case,[23] there is a gradient of degree of oxidation from the surface inward when O_2 evolution rate is increased or in the reverse direction when it is decreased. The self-discharge process is then accompanied by a 'diffusion of state of oxidation',[5] associated with proton and electron migration in the hydrous oxide. This provides a coupling of the density of surface-state intermediates in the o.e.r. to the redox state of the underlying bulk oxide of the film [*cf.* process (2)].

Effects of Temperature

Effects of temperature in electrocatalysis are usually of substantial practical and sometimes theoretical interest,[31] although it is well known that only apparent heats of activation for electrode processes are directly accessible from experimental data. Nevertheless, results for comparative behaviour over a range of temperatures are useful, *e.g.* as found for other processes treated in recent papers,[7, 9, 31] especially with regard to the temperature dependence of the transfer coefficient.[31] Results of polarization and potential-decay measurements are shown in fig. 8 and 9 for three temperatures 273.6, 299.1 and 338.1 K. The data are processed as described earlier and give rise to the plots of η *vs.* $\log(-\mathrm{d}\eta/\mathrm{d}t)$ and C *vs.* η as shown in fig. 10 and 11, respectively, for the three or two temperatures. The V *vs.* $\log(-\mathrm{d}\eta/\mathrm{d}t)$ plots for 273.6 and 299.1 K lie parallel to each other, and both exhibit an inflected line with two slopes having values of 26–30 and

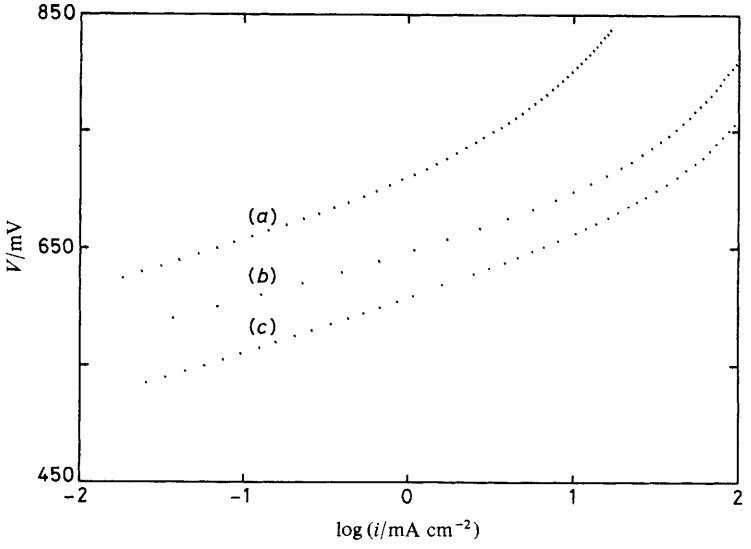

Fig. 8. Tafel relations for O_2 evolution at oxidized Ni electrodes in 0.2 mol dm^{-3} at three temperatures: (*a*) 273.6 K (b_T = 44 mV), (*b*) 299 K (b_T = 39 mV) and (*c*) 338 K (b_T = 44 mV).

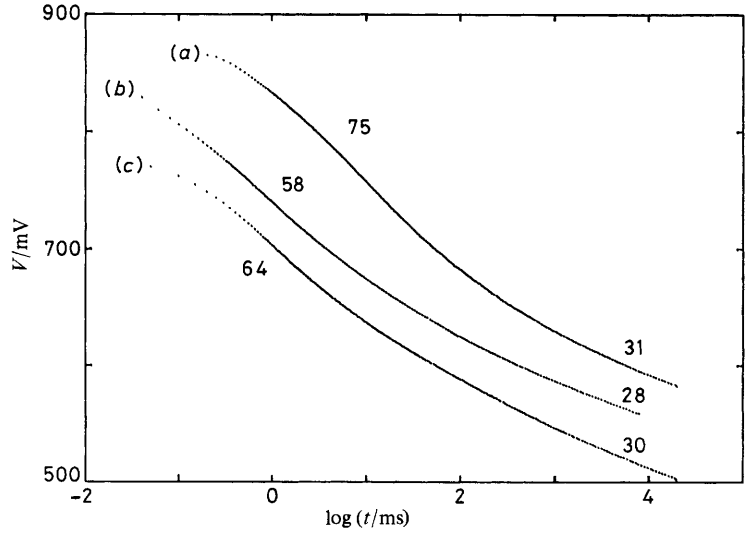

Fig. 9. Potential decay transients, digitally recorded, plotted *vs.* log time for the three temperatures corresponding to the results in fig. 8: (*a*) 273.6 K from 53 mA cm^{-2}, (*b*) 299 K from 104 mA cm^{-2} and (*c*) 338 K from 55 mA cm^{-2}. Values of b_t/mV as shown on the curves.

39–47 mV, virtually independent of temperature. The capacitance in the intermediate region (fig. 11) lies lower at lower temperature (273.6 K) than at higher (299.1 K).

The Tafel plots (fig. 8) are shifted towards higher current densities, at given overpotentials, as the temperature is increased, as expected. The Tafel slopes increase with temperature in the conventional ($b = \boldsymbol{RT}/\alpha\boldsymbol{F}$) (but not always observed[31]) way.

From the $C_\phi + C_{dl}$ *vs.* η plots for the behaviour of the OH or O intermediates at two

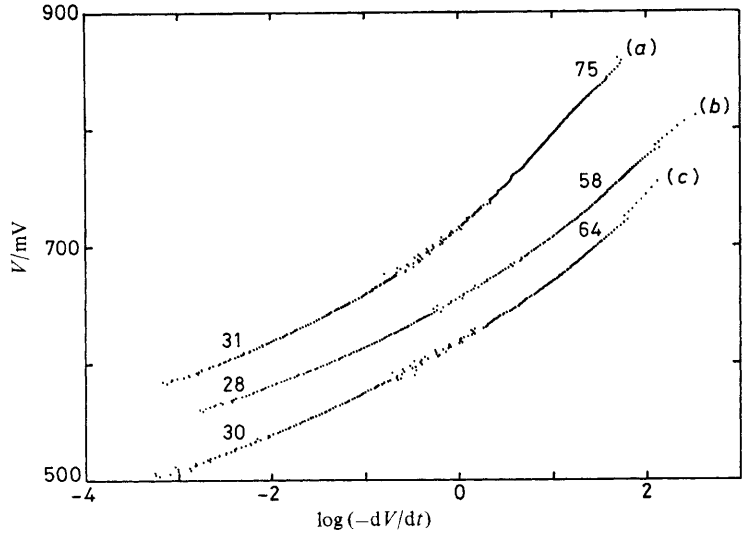

Fig. 10. Plots of electrode potential *vs.* $\log(-\mathrm{d}V/\mathrm{d}t)$ from the potential decay data shown in fig. 9: (*a*) 273.6, (*b*) 299 and (*c*) 388 K. Values of *d* as shown on the curves.

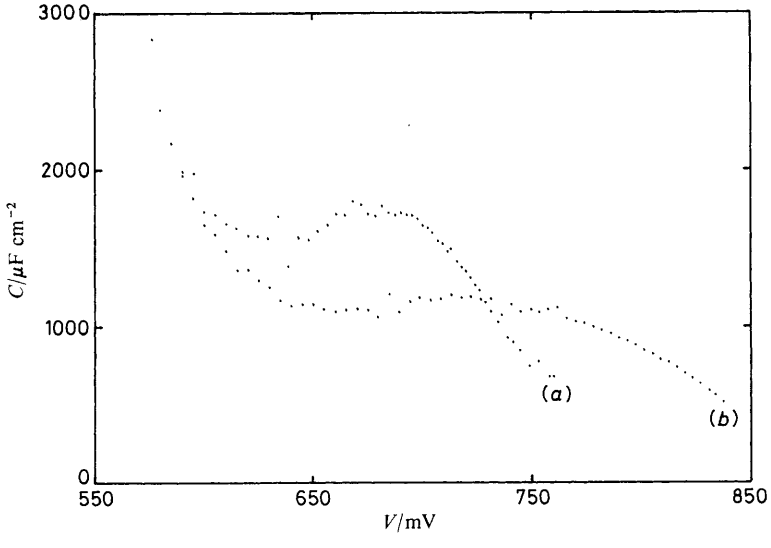

Fig. 11. Plots of $C_\phi + C_{\mathrm{dl}}$ as a function of potential, as in fig. 7(*b*), but for the two temperatures: (*a*) 299 and (*b*) 273.6 K.

temperatures (fig. 11) it is possible to derive the corresponding Δq (see previous section and fig. 7) *vs.* η plots. These were shown in fig. 7(*b*). At the lower temperature of 273.6 K, a higher potential is required for a given value of Δq to be attained than that for 299.1 K. The difference is a large one (110 mV for $\Delta q = 200\ \mu\mathrm{C\ cm^{-2}}$, say) and therefore must represent a kinetic rather than a thermodynamic effect. This is as expected, since Δq and the corresponding C_ϕ represent quantities having a kinetic significance rather than a thermodynamic one, connected with the behaviour of intermediates in the course of

Table 1. Relation between Tafel slope, b, and potential-decay slope functions, b_t and d, in mV at 299 K

Tafel slope, b		$b_t = dV/d\log(t+\tau)$		$d = dV/d\log(-dV/dt)$	
upper	lower	upper	lower	upper	lower
$\geqslant 65^a$	37	−58	−28	58	28

[a] Curving region after 'iR' correction (fig. 2).

the reaction at various net current densities (*cf.* the difference between the steady-state pseudocapacitance[26c] and the equilibrium quantity observable in u.p.d. experiments[10, 11, 26b]). Similar sensitive dependence of C_ϕ for adsorbed H species on temperature was observed recently[7] in our studies of the H_2 evolution reaction on Ni, where the H coverage behaviour depends on the ratio of rate constants for H deposition and desorption and on potential.

Slopes of Tafel and Potential Decay Relations in $\log t$ and $\log(-d\eta/dt)$

Fig. 9 and 10 show the same potential-decay data for three temperatures plotted out according to the integration of eqn (1) [$\eta(t)$ *vs.* $\log t$ or $\log(t+\tau)$] or directly in differential fashion [$\eta(t)$ *vs.* $\log(-d\eta/dt)$]. Each of these plots has two regions of different slope (28–31 and 58–75 mV per decade), but the two types of plots have numerically the same slopes for the respective two regions. This is as expected since $d\eta/d\ln t = t(d\eta/dt) = K$ (a constant) for a given region and for $t \gg \tau$. Also, therefore, $\ln(-d\eta/dt) = \ln(-K) - \ln t$; then differentiating with respect to η gives $d\ln(-d\eta/dt) = -d\ln t/d\eta$, so that the slopes of $\eta(t)$ *vs.* $\ln t$ or $\ln(t+\tau)$ and $\eta(t)$ *vs.* $\log(d\eta/dt)$ plots are expected to be equal but of opposite sign, as observed over both regions of the potential-decay range.

It is of interest to show how the profile of C with respect to potential, derived using eqn (1) (see section containing fig. 6), is related to the shape of the Tafel curve for a typical temperature, 299 K: fig. 2 shows $C(V)$ superimposed on the $\ln i(V)$ relation. The most rapidly changing region of $C(V)$ [$C(V)$ decreasing with increasing anodic potential] corresponds to the low-slope regions of the Tafel relations (b_T = 39–44 mV, depending on temperature—see fig. 8). This region of the $C(V)$ profile seems to correspond with the pseudocapacitance associated with the potential dependence of the degree of oxidation of the bulk nickel oxide material just before, or at, the potential for commencement of significant rates of O_2 evolution, as indicated by the rising current region of the cyclic voltammogram of fig. 1 just below (less positive than) 0.589 V *vs.* Hg/HgO, which corresponds to the rising region of $C(V)$ in fig. 2 or 6 below $V \approx 600$ mV *vs.* Hg/HgO.

Between *ca.* 0.625 and 0.690 V a region of little varying C arises, with a descent to lower values beyond 0.690 V (fig. 2), corresponding to the range of V where the iR-corrected Tafel slope increases to 58–65 mV.

Unlike the analysis we were able to make[7] for o.p.d. H adsorption in the H_2 evolution reaction at Ni and Ni—Mo—Cd electrodeposits, it is not possible to make a significant plot of C *vs.* V here owing to the evidently more complex variation of C with V seen in fig. 2 or 6, which, it may be suggested, is due to overlap of pseudocapacitance contributions from the potential dependence of the oxidation state of the bulk phase 'Ni·O·OH',[32] and from potential dependence of the surface density of extra OH species or corresponding Ni^{IV} states as the potential is raised above *ca.* 0.59 V (at 299 K).

The Tafel relations (fig. 2 and 8) have a slope of 39–44 mV at the lower current density ends and a smoothly increasing slope above potentials of 0.58 or 0.63 V at 299 and 273.6 K, respectively, to values of *ca.* 58–65 mV. The observation of low Tafel slopes coupled with appreciable pseudocapacitance of the intermediates implies that a desorption step is rate-controlling with potential dependence of the coverage by, or surface density of, the intermediates [see process (2)]. Through arguments given elsewhere,[7, 22] since the potential-decay slopes of the $\log(t+\tau)$ plots are significantly less than the numerical values of the Tafel slopes over the respective potential ranges, it follows that the pseudocapacitance of the adsorbed intermediates increases with decreasing potential. This is as deduced directly from eqn (1), giving the plots of fig. 7 or 11 for the capacitance which, as we have remarked earlier, increases rather rapidly below *ca.* 0.57 V, in fact in an approximately exponential manner with decreasing potential.

Taking the logarithm of eqn (1), it is seen that the slope $[\mathrm{d}\ln(-\mathrm{d}\eta/\mathrm{d}t)]/\mathrm{d}\eta$ of the $\ln(-\mathrm{d}\eta/\mathrm{d}t)$ *vs.* η plot can be expressed as

$$\frac{\mathrm{d}\ln(-\mathrm{d}\eta/\mathrm{d}t)}{\mathrm{d}\eta} = \frac{1}{b_\mathrm{T}} - \frac{1}{b_\mathrm{C}} = \frac{1}{d} \tag{2}$$

say, where b_T is the Tafel slope $\mathrm{d}\eta/\mathrm{d}\ln i$ and b_C is the slope of the dependence of $\ln C$ on η when C is $f(\eta)$, *i.e.* usually when $C_\phi \gg C_{\mathrm{d}1}$. Thus d differs from b_T for the same reason that the logarithmic decay slope $\mathrm{d}\eta/d\ln(t+\tau)$ differs from $-b_\mathrm{T}$.

The results shown in fig. 2, 3(*b*) and 4 can be tested against eqn (2) to estimate b_C, assuming there may be a dependence of C on η over the lower overpotential range where $b_\mathrm{T} = 37 \pm 1$ mV, and the decay slope $|b_\mathrm{t}|$ and the slope d are each 28 ± 1 mV at 299 K (table 1). Evaluating b_C from eqn (21) we then find $\mathrm{d}\log C/\mathrm{d}\eta = 1/b_\mathrm{C} = -8.7$ or $b_\mathrm{C} = -114 \pm 2$ mV. Thus C decreases with increasing η, as is consistent with the behaviour in fig. 2 for the low-overpotential region. For the higher-overpotential region, where an ill-defined Tafel slope of *ca.* 65 ± 5 mV seems to arise, the b_T and d slopes are in the range 47–59 mV, indicating (in comparison with the b_t value) a less sensitive dependence of C on potential. This is supported qualitatively by the C *vs.* potential profiles of fig. 2 or 6, where C appears to decrease more or less linearly with potential in the upper potential region (+0.690 to 0.750 V). The value, *ca.* −114 mV, for $\mathrm{d}\eta/\mathrm{d}\log C$ is not easy to account for as it is near $-2.3 \times 2\boldsymbol{RT}/\boldsymbol{F}$ rather than $-2.3\boldsymbol{RT}/\boldsymbol{F}$, which would be easier to understand. It suggests, however, an expected irreversibility in the deposition and desorption of the intermediates at appreciable current densities.

Formally, a Tafel slope of *ca.* 59 mV at 299 K implies a one-electron quasiequilibrium prior to a 'chemical' rate-controlling step of the first order. (A two-electron step with a common transition state, which would lead to the same result, is generally considered unlikely in electrode kinetics.) The lower Tafel slope of 39–44 mV, depending on temperature, is near to the value expected (39 mV at 298 K) for a one-electron quasiequilibrium prior to a second-order rate-controlling electrochemical desorption step, *i.e.* with $\alpha = 1.5$.

At the potentials where appreciable rates of O_2 evolution arise (*cf.* fig. 1), it is likely that the step which determines the state of the nickel oxide surface is

$$\mathrm{Ni^{III}{\cdot}O{\cdot}OH + OH^- \rightarrow Ni^{IV}{\cdot}O{\cdot}O + H_2O + e}$$

but with a surface density of Ni^{IV} states well below that corresponding to complete conversion of Ni^{III} to Ni^{IV}. It is not easy to identify the first-order chemical step required for a mechanism giving rise to a 59 mV slope except perhaps the reaction

$$\mathrm{2Ni{\cdot}O{\cdot}O + H_2O \rightarrow 2Ni{\cdot}O{\cdot}OH + \tfrac{1}{2}O_2}$$

which could be kinetically first-order through the Ni^{4+} states in the surface, *i.e.* the decomposition of the H_2O by the Ni^{IV} oxide states. Surface diffusion of active intermediate species, Ni^{IV} or O, from one site on the surface to a preferred reaction site

nearby, is another possibility but, we believe, less likely. A 59 mV slope may also arise, according to ideas of Krishtalik, on account of 'barrierless discharge', but this case is unlikely to apply here since, towards lower overpotentials, the slope decreases from *ca.* 59 to *ca.* 32 mV rather than increasing to 118 mV (symmetry factor changing from 1 to *ca.* 0.5) in the way expected for such an effect.

Conclusions

Quantitative processing of digitally acquired potential-decay transients, coupled with information from Tafel polarization lines, enables changes of coverage and associated pseudocapacitance with potential to be evaluated for the kinetically involved intermediates in the anodic O_2 evolution reaction at oxidized Ni electrodes. It is suggested that the intermediates are OH and O species associated with Ni ion in the surface of the oxide film lattice in oxidation states corresponding to Ni^{3+} and Ni^{4+}, depending on electrode potential and O_2 evolution rate.

Two regions of the capacitance behaviour observed as a function of potential can be distinguished: one probably associated with changing oxidation state of bulk oxide in the film, coupled with the oxidation state of the surface, and the other reflecting, over a broader potential range, the change of oxidation state of Ni ion species on the surface of the oxide film, associated with adsorbed OH and O intermediates in the oxygen evolution process.

The pseudocapacitance behaviour of the adsorbed intermediates in the o.e.r. is quite sensitive to change of temperature. This is understood in terms of the kinetic, rather than thermodynamic, significance of the C_ϕ quantity that is determined in the experiments on potential decay from appreciable overpotentials where substantial currents were previously passing.

Grateful acknowledgment is made to the Natural Sciences and Engineering Research Council of Canada for support of this work. T. L. acknowledges award of an advanced study leave from the People's Republic of China during 1984 and 1985.

References

1 J. A. V. Butler, *Proc. R. Soc. London, Ser. A*, 1936, **157**, 423.
2 J. Horiuti and M. Polanyi, *Acta Physicochim. U.R.S.S.*, 1935, **2**, 505.
3 J. O'M. Bockris, *J. Chem. Phys.*, 1956, **24**, 817.
4 B. E. Conway, in *MTP International Review of Science, Ser. 1, Vol. 6: Electrochemistry*, ed. J. O'M. Bockris (Butterworths, London, 1973), chap. 2, p. 41.
5 B. E. Conway and P. L. Bourgault, *Can. J. Chem.*, 1959, **37**, 292.
6 S. Trasatti, *J. Electroanal. Chem.*, 1980, **111**, 125; see also A. C. C. Tseung, *Electrochim. Acta*, 1977, **22**, 31.
7 B. E. Conway and L. Bai, *J. Chem. Soc., Faraday Trans. 1*, 1985, **81**, 1841.
8 J. O'M. Bockris, in *Modern Aspects of Electrochemistry*, ed. J. O'M. Bockris (Butterworths, London, 1954), vol. 1, chap. 4.
9 B. E. Conway and L. Bai, *Proc. 5th World Hydrogen Energy Conference*, Toronto, Canada, 1984 (Pergamon Press, New York, 1985), pp. 879–889.
10 F. G. Will and C. A. Knorr, *Z. Elektrochem.*, 1960, **64**, 270.
11 K. Engelsman, W. J. Lorenz and E. Schmidt, *J. Electroanal. Chem.*, 1980, **114**, 1.
12 K. J. Vetter and D. Berndt, *Z. Elektrochem.*, 1958, **62**, 378.
13 K. J. Vetter and J. W. Schultze, *Ber. Bunsenges. Phys. Chem.*, 1971, **75**, 470; 1969, **73**, 483.
14 M. W. Breiter, H. Kammermaier and C. A. Knorr, *Z. Elektrochem.*, 1956, **60**, 37.
15 M. W. Breiter, C. A. Knorr and W. Völkl, *Z. Elektrochem.*, 1955, **59**, 681.
16 H. Gerischer and W. Mehl, *Z. Elektrochem.*, 1955, **59**, 1049.
17 J. O'M. Bockris, M. A. V. Devanathan and W. Mehl, *J. Electroanal. Chem.*, 1959, **1**, 143.
18 B. E. Conway and L. Bai, *J. Electroanal. Chem.*, 1986, **198**, 149.
19 B. E. Conway and L. Bai, *Electrochim. Acta* (Proc. 3rd Fischer Symposium, Karlsruhe, 1985), 1986, **31**, 1013.
20 B. E. Conway and P. L. Bourgault, *Trans. Faraday Soc.*, 1962, **58**, 593.

21 H. B. Morley and F. E. W. Wetmore, *Can. J. Chem.*, 1956, **34**, 359.
22 B. V. Tilak and B. E. Conway, *Electrochim. Acta*, 1976, **21**, 745.
23 H. Willems, A. G. C. Kobussen, I. C. Vinke, J. H. W. de Wit and G. H. J. Broers, *J. Electroanal. Chem.*, 1985, **194**, 287.
24 H. Willems, A. G. C. Kobussen and J. H. W. de Wit, *J. Electroanal. Chem.*, 1985, **194**, 317.
25 J. A. V. Butler and J. F. Armstrong, *Trans. Faraday Soc.*, 1933, **29**, 1261.
26 *E.g.* see (*a*) A. Eucken and B. Weblus, *Z. Elektrochem.*, 1951, **55**, 114; (*b*) B. E. Conway and E. Gileadi, *Trans. Faraday Soc.*, 1962, **58**, 2493; (*c*) *J. Chem. Phys.*, 1963, **39**, 3420.
27 B. E. Conway, L. Bai and D. Tessier, *J. Electroanal. Chem.*, 1984, **161**, 39.
28 A. G. C. Kobussen, H. Willems and G. H. J. Broers, *J. Electroanal. Chem.*, 1982, **142**, 67.
29 D. A. Harrington and B. E. Conway, *J. Electroanal. Chem.*, in press.
30 B. E. Conway and P. L. Bourgault, *Can. J. Chem.*, 1962, **40**, 1690.
31 B. E. Conway, D. J. MacKinnon and B. V. Tilak, *Trans. Faraday Soc.*, 1970, **66**, 1203; see also B. E. Conway, in *Modern Aspects of Electrochemistry*, ed. B. E. Conway, J. O'M. Bockris and R. E. White (Plenum, New York, 1985), vol. 16, chap. 2.
32 J. Weininger and M. W. Breiter, *J. Electrochem. Soc.*, 1963, **110**, 484; 1964, **111**, 707.

Paper 6/818; *Received* 28*th April*, 1986